Microvascular maturation by mesenchymal stem cells in vitro improves blood perfusion in implanted tissue constructs

Yoann Atlas, Caroline Gorin, Anita Novais, Marion F. Marchand, Eirini Chatzopoulou, Julie Lesieur, Rumeyza Bascetin, Clément Binet-Moussy, Jeremy Sadoine, Matthieu Lesage, et al.

Microvascular maturation by mesenchymal stem cells *in vitro* improves blood perfusion in implanted tissue constructs

Yoann Atlas[1,2,*], Caroline Gorin[3,4,*], Anita Novais[3,4,*], Marion F. Marchand[1,2], Eirini Chatzopoulou[3,4], Julie Lesieur[3], Rumeyza Bascetin[1,+], Clément Binet-Moussy[1], Jeremy Sadoine[3], Matthieu Lesage[1], Sibylle Opsal-Vital[3,4], Bruno Péault[5,6], Catherine Monnot[1], Anne Poliard[3], Philippe Girard[7], Stéphane Germain[1,#], Catherine Chaussain[3,4,#,Δ], Laurent Muller[1,#,Δ]

1: Center for Interdisciplinary Research in Biology (CIRB), College de France, CNRS UMR7241, INSERM U1050, PSL Research University, Paris, France
2: Sorbonne Université, Collège doctoral, Paris, France
3: Université de Paris, UR2496 Pathologies, Imagerie et Biothérapies Orofaciales et Plateforme Imagerie du Vivant, Paris, France
4: AP-HP, Services Odontologie (GH Paris Est, Paris Nord, Henri Mondor), France
5 : Department of Orthopaedic Surgery, UCLA and Orthopaedic Hospital, Orthopaedic Hospital Research Center, Los Angeles, United States
6: Center for Cardiovascular Science, MRC Center for Regenerative Medicine, University of Edinburgh, Edinburgh, United Kingdom
7: Institut Jacques Monod, UMR7592 CNRS, Université de Paris, Paris, France

[*] and [#]: Contributed equally to this work.

[Δ] : Corresponding Authors: Laurent Muller, PhD, Center for Interdisciplinary Research in Biology, College de France, Paris, 11 Place Marcelin Berthelot, F-75005, France. +33(0)144271429. FAX. +33(0)144271691; email : laurent.muller@college-de-france.fr and Catherine Chaussain, DDS-PhD, UR2496, Université de Paris, 1 rue Maurice Arnoux 92120 Montrouge, France ; Tel and Fax : +33(0)158076724; email: catherine.chaussain@u-paris.fr

[+] Present address : Fonds de la Recherche Scientifique (F.R.S./FNRS), Université Libre de Bruxelles, Gosselies, Belgium

SHORT TITLE: Microvascular maturation *in vitro* improves blood perfusion *in vivo*

Keywords: Dental pulp stem cells, angiogenesis, vascular niche, perivascular recruitment, basement membrane

ABSTRACT

Blood perfusion of grafted tissue constructs is a hindrance to the success of stem cell-based therapies by limiting cell survival and tissue regeneration. Implantation of a pre-vascularized network engineered *in vitro* has thus emerged as a promising strategy for promoting blood supply deep into the construct, relying on inosculation with the host vasculature. We aimed to fabricate *in vitro* tissue constructs with mature microvascular networks, displaying perivascular recruitment and basement membrane, taking advantage of the angiogenic properties of dental pulp stem cells and self-assembly of endothelial cells into capillaries. Using digital scanned light-sheet microscopy, we characterized the generation of dense microvascular networks in collagen hydrogels and established parameters for quantification of perivascular recruitment. We also performed original time-lapse analysis of stem cell recruitment. These experiments demonstrated that perivascular recruitment of dental pulp stem cells is driven by PDGF-BB. Recruited stem cells participated in deposition of vascular basement membrane and vessel maturation. Mature microvascular networks thus generated were then compared to those lacking perivascular coverage generated using stem cell conditioned medium. Implantation in athymic nude mice demonstrated that *in vitro* maturation of microvascular networks improved blood perfusion and cell survival within the construct. Taken together, these data demonstrate the strong potential of *in vitro* production of mature microvasculature for improving cell-based therapies.

(211 words)

INTRODUCTION

Tissue engineering is now considered as the novel route for replacing or supporting regeneration of failing organs by providing large enough and function-relevant constructs consisting in scaffolds seeded with cells. The success of this strategy is directly conditioned by the establishment of a fully functional microvascularization in order to support cell survival and differentiation [1,2]. Indeed, blood supply must be established both rapidly and deep inside the grafted engineered construct to provide oxygen and nutrients. Promoting angiogenesis *in situ* is often not appropriate to fulfill these criteria; notably in the case of delayed wound healing found in patients suffering from diabetes or metabolic syndrome, or in smokers. Hence, pre-vascularization of tissue constructs appears as a promising approach consisting in implantation of engineered microvascular networks developed *in vitro* with the aim of allowing blood perfusion at once deep in the implanted construct [3]. Perfusion of the implanted network then relies on anastomosis with the host vasculature [4–8].

In this context, it appears mandatory to identify both molecular and cellular targets, and key mechanisms to enhance vascular network formation *in vitro* [3,9]. Microvascular networks can be developed *in vitro* based on the capacity of endothelial cells to self-assemble into capillary structures in the appropriate culture conditions. Such a process mimics vasculogenesis that occurs during development and is completed by sprouting angiogenesis as tissues grow. Both processes are accompanied by remodeling of the microenvironment and generation of the vascular basement membrane [10]. Hydrogels of natural polymers are considered more prone to support such remodeling and cell function associated with *in vitro* pre-vascularization and integration in the host after implantation. Fibrin and collagen I are the two main sources of natural polymers suitable for development of microvascularization. Whereas fibrin is very susceptible to degradation with a rate of replacement often too high for efficient tissue repair, collagen I is extensively used and better suited to cell self-assembly approaches [11]. The use of stem cells able to promote both tissue regeneration and angiogenesis in collagen hydrogels appears as an appealing option for productive pre-vascularization. Angiogenesis is initiated in response to local production of proangiogenic factors that promote vascular sprout formation through induction and migration of leading endothelial tip cells and proliferation of neighboring endothelial stalk cells [12]. This process is promoted by mesenchymal stem cells (MSC). Dental pulp stem cells (DPSC) have been described as an accessible source of MSC for tissue engineering, able to differentiate within various lineages according to the environment they are placed to [13–15]. Healthy dental pulps can be collected in patients from shedding deciduous teeth, or following extraction of deciduous teeth, premolars or third molars strictly performed when indicated in an orthodontic treatment plan (waste of the operating room). Many preclinical studies have revealed the interest of DPSC for regenerative medicine [16] and recently, Nakashima et al. published a pilot clinical study showing the benefit of the use of autologous DPSC for complete tooth pulp regeneration in patients with irreversible pulpitis [17] [18]. More recently, it was demonstrated in 36 young patients with injured immature permanent tooth following a trauma that aggregates of DPSC derived from deciduous teeth (SHED) improved pulp healing and allowed normal tooth formation[19]. We and others have shown their capacity to induce capillary formation *in vitro* through the release of angiogenic factors [20–22]. Along this line, we have recently shown that FGF-2-priming of DPSC seeded in a collagen hydrogel enclosed in a tooth slice allowed the formation of a functional vascularized pulp-like tissue upon sub-cutaneous implantation

in immunodeficient mice [22]. Using relevant 3D angiogenesis models, we could decipher the signaling cascade involved consisting in FGF-2 stimulation of DPSC to release VEGF that induces capillary formation, and HGF that potentiates VEGF effect on endothelial cells [22].

Other important steps of neovessel formation include perivascular recruitment of pericytes by endothelial sprouts and basement membrane deposition [12]. Endothelial cells and pericytes share a common basement membrane and communicate with each other via physical contact and paracrine signaling pathways thus promoting vascular maturation and regulation of vascular permeability and integrity [23,24]. MSC and pericytes are known to share perivascular distribution and regeneration properties [25,26]. Indeed, DPSC are located in the vascular niche and were proposed to have pericyte-like properties [27,28]. These cells have also been shown to present an immunophenotypic pericyte profile that depended on the isolation method and culture conditions [22,28,29]. The aim of the present study was thus: -1/ to generate pre-vascularized constructs co-seeded with endothelial cells and DPSC derived from deciduous teeth (SHED); -2/ to characterize interactions between these two cell types and unravel molecular pathways involved in capillary formation and maturation; -3/ to assess the impact of *in vitro* vascular maturation on the integration of the tissue constructs after implantation. Using 3D co-culture models, we report that SHED were recruited to the capillary surface and extended protrusions enwrapping endothelial cells. We could characterize morphometric parameters associated with their recruitment through the PDGF-BB signaling pathway, and demonstrate that once recruited, SHED participated in basement membrane generation. Furthermore, we showed that ectopic subcutaneous implantation of such mature microvascular networks resulted in better vascularization, protection from apoptosis and innervation.

RESULTS

- ***In vitro* generation of microvascular networks with perivascular cell recruitment in 3D hydrogels**

We have already demonstrated that the angiogenic potential of SHED relies on the paracrine factors VEGF and HGF, resulting in formation of lumenized capillaries in 3D hydrogels [22]. We here took advantage of these properties for generating dense homogenous microvascular networks in collagen hydrogels. Endothelial cells (1.5 x 10^6 cells/ml) were seeded in collagen hydrogels either alone before cultured in SHED-conditioned medium or together with 1 x 10^6 SHED/ml before co-culture for 4 days in 96 well plates (Fig. 1A). Microvascular networks were analyzed in 3D using an in-house developed software called 3D-Skel (Fig. S1). Both conditions resulted in microvascular networks reaching an average of 80 mm of capillaries per mm^3 of hydrogel. The extent of these networks was only 12% higher in conditioned medium renewed every day than in co-culture, with identical tortuosity and diameter of the capillaries (Fig. 1B). In order to further characterize the cell interactions occurring in co-culture, SHED expressing LifeAct-Ruby were co-seeded in collagen with endothelial cells expressing GFP. After 4 days in co-culture, gels were fixed and embedded in agarose for observation on an in-house built digital scanned light-sheet microscope (DSLM) (Fig. 1C). The fields of view were 665 x 665 µm, and images were acquired over a thickness of 400 µm with 1 µm steps (Fig. 1D, movie 1). 3D analysis of SHED distribution and morphology revealed that these cells displayed either a star-shaped morphology when isolated in the hydrogel (red in Fig. 1D and E) or had acquired a fine elongated structure spread along endothelial cells, with protrusions wrapped around the capillaries (purple in Fig. 1D-F and movie 1), suggesting a morphological change associated to dynamic perivascular cell recruitment. In addition, we could detect lumen formation in the capillaries, including at the level of perivascular SHED, using higher magnification microscopy (Fig. 1F; movie 2), supporting functionality and blood perfusion of such capillaries after post-implantation inosculation.

In order to analyze perivascular recruitment of SHED, we investigated the expression of some markers of perivascular cells. SHED did not express alpha smooth muscle actin (aSMA), whereas a mosaic expression was detected in pericytes, with the highest signal still much lower than in vascular smooth muscle cells (Fig. 2A). SHED expressed similar levels of desmin, NG2 and PDGF-Rβ as pericytes (Fig. 2 B-C). We also investigated the expression of the latter in co-culture with endothelial cells in 3D hydrogels. We did not detect differences in PDGF-Rβ expression level whereas SHED were associated to endothelial cells or not (Fig. 2D; movie 3). Since we lacked immunological marker enabling identification of SHED recruited to the vascular niche, we characterized morphometric parameters for assessment of their recruitment. For that purpose, we measured the distance between the centroid of SHED nuclei and the surface of endothelial capillaries (Fig. 3A) using Imaris (Fig. S1). Distances were then correlated to SHED morphology as assessed by two independent observers. This analysis was performed using measurements from 5 stacks of images from 3 independent culture hydrogels, for a total of 735 SHED with nuclei at a distance under 16 µm from the endothelium: 88 % of the cells with nuclei at less than 9 µm displayed a perivascular morphology, while 89% of the cells with nuclei further than 9 µm had a star-shaped morphology (Fig. 3B). We also performed time-lapse acquisitions to analyze the behavior of SHED upon recruitment to the

endothelium (Fig. 3C and movie 4). For these experiments, the smallest possible chamber was constructed and precise temperature control was achieved by using a Peltier element located under the chamber and by including the whole microscope in a temperature-controlled incubator (Fig. S2A-B). We built a sample holder dedicated to hydrogels that could support casting of cellularized hydrogels and early culture in an incubator before mounting on the DSLM without manipulation of the hydrogel (Fig. S2C). After three days of culture for capillary formation, hydrogels co-seeded with SHED expressing LifeAct-Ruby and endothelial cells expressing GFP were mounted on the DSLM for time-lapse acquisitions over a period of 7 hours (Fig.3C and movie 4). While most of the SHED present as isolated cells in the collagen hydrogel were mobile (red in movie 4), two behaviors were observed for SHED associated with capillaries. Those already recruited to capillaries at the beginning of the time-lapse acquisition were quite static (purple in fig. 3C and movie 4). In contrast, SHED recruited in the course of the time-lapse acquisition were very mobile, migrating along the endothelium (colored in white in Fig. 3C and movie 4). We could thus separate SHED into two populations, recruited or not to capillaries, with a morphometric threshold that allowed automated quantitation. Thirty percent of SHED were recruited as perivascular cells 3 days after seeding the ratio of 1.5:1 endothelial cells: SHED. Using different ratios of SHED: endothelial cells and different total numbers of cells suggested that the extent of the capillary network was increased by both factors (Fig. S3A). On the other hand, only cell ratio could modulate SHED recruitment, entailing that the density of SHED in the capillary network formed was a limiting factor to perivascular cell recruitment (Fig. S3B). These data suggested that exposure of SHED to a paracrine endothelial factor is responsible for perivascular recruitment.

- **Perivascular recruitment of SHED through the PDGF-BB pathway**

Pericyte recruitment by the PDGF-BB/PDGF-Rβ signaling pathway has been extensively documented [23,24] and could be mimicked in 3D hydrogels using gradients of this growth factor [30]. Considering the expression of PDGF-Rβ by SHED, we investigated the hypothesis that PDGF-BB secreted by endothelial cells is responsible for SHED recruitment in the hydrogel. For that purpose, we adapted an angiogenesis assay based on seeding endothelial cells at the surface of Cytodex beads [31,32] and on co-incorporating these beads together with SHED in the hydrogel before fibrillogenesis (Fig. 4A; movie 5). This co-culture model allowed to measure the number of SHED recruited per length of capillary generated, and thus to compare the impact of treatments on capillary formation and on perivascular recruitment. We first inhibited PDGF-Rβ tyrosine kinase activity with Imatinib, which did not significantly affect the length of capillaries per bead but however inhibited perivascular recruitment in a dose-dependent manner (Fig. 4B and D). A second approach targeted the PDGF secreted by endothelial cells using: -i/ heparin, which captures factors that bind heparan sulfate proteoglycans, including PDGF-BB [33]; -2/ a blocking antibody specific for PDGF. Heparin inhibited angiogenesis by 20% and perivascular recruitment by 70%, whereas anti-PDGF had a dose-dependent effect on perivascular recruitment, which was inhibited up to 50% (Fig. 4B and D). The absence of correlation between the expression of PDGF-Rβ by SHED and their recruitment (Fig. 2D; movie 3) supports the hypothesis that it is exposure of SHED to the gradient of PDGF secreted by endothelial cells that triggers recruitment rather than expression of the receptor. To explore this hypothesis, we used a complementary approach consisting in disrupting the gradient that is generated by secretion of PDGF-BB and sequestration by heparan sulfate proteoglycans in the

vicinity of endothelial cells. For that purpose, we added exogenous PDGF-BB to the culture medium. A dose twice the ED_{50} (10 ng/ml) had no effect on angiogenesis and perivascular recruitment, while it was expected to be high enough for stimulating cell migration. More importantly, adding 100 ng/ml PDGF-BB resulted in 65% inhibition of SHED recruitment instead of stimulating their migration and thus their potential recruitment. This high dose of PDGF-BB also slightly inhibited capillary formation (Fig. 4B and D). Similar results were obtained using human primary pericytes isolated from the placenta (Fig. S4). Altogether, these three independent approaches demonstrated that SHED are recruited to the vascular niche through the PDGF signaling pathway.

- **SHED perivascular recruitment promotes capillary maturation**

Generation of a basement membrane that encompasses both the endothelium and the associated perivascular cells is involved in maturation and stabilization of capillaries [23,34]. We therefore studied deposition of type IV collagen in the 3D culture hydrogel (Fig. 5A). In addition to deposition at the surface of endothelial cells, we also detected collagen IV ensheathing perivascular SHED recruited along capillaries (Fig. 5Aii, yellow arrow; movie 6). In order to investigate whether SHED participated in the generation of the capillary basement membrane, we cultivated these cells beyond confluency in tissue culture dishes to accumulate matrix deposition. Whereas no collagen IV was deposited when SHED were cultured in their dedicated culture medium, the medium used in the vascularization assay induced collagen IV deposition (Fig. 5B). The increased deposition of collagen IV did not result from increased expression, but from post-translational mechanisms initiated by the increased expression of laminin (fig.S5A), which acts as a foundational building block for deposition of collagen IV and further organization of the basement membrane [35]. Unlike SHED, primary human pericytes could deposit collagen IV when cultured in their dedicated culture medium without growth factor supplement, and endothelial cells conditioned medium increased this deposition (Fig. S5B). These data suggested that growth factors present in the endothelial culture medium could promote collagen IV secretion and assembly by SHED, and demonstrated co-ensheathing of endothelial cells and perivascular SHED in the vascular basement membrane of the capillaries generated *in vitro*. Taken together, our *in vitro* results demonstrated that SHED could trigger formation of a microvascular network through paracrine factors and participate in the two major aspects of the maturation of capillaries, i.e. perivascular cell recruitment and deposition of the vascular basement membrane.

- **Blood perfusion is enhanced in pre-vascularized tissue constructs**

In order to investigate the impact of pre-vascularizing constructs on their *in vivo* perfusion, we used a previously described model of tooth slice subcutaneous implantation in athymic NUDE mice [22]-[36]. Pre-vascularized hydrogels were compared to hydrogels seeded with SHED alone and cultured in the same conditions prior to implantation. Furthermore, pre-vascularized hydrogels were generated either by co-seeding endothelial cells and SHED or by seeding endothelial cells alone, in order to assess the impact of *in vitro* microvascular maturation by SHED. When seeded with endothelial cells alone, hydrogels were cultured with SHED conditioned medium, as co-culture and conditioned medium generated microvascular networks that were equivalent at the time of implantation (Fig. 1A). Angiogenesis was explored 30 days after implantation by micro-CT analysis

following intracardiac injection of a contrast agent, and then further characterized by histology and immunohistochemistry. Micro-CT acquisitions revealed significantly higher vascular perfusion in the pre-vascularized groups when compared to the SHED control group ($P \leq 0.05$) (Fig. 6A-B). Immunohistochemical labelling performed using a von Willebrand factor (vWF) antibody, confirmed the benefit of pre-vascularization on capillary density in the constructs and indicated a much higher impact of the implantation of a mature microvascular network (Fig. 6C and D). These data were further confirmed using a podocalyxin antibody that is specific for the human protein (Fig.6E and F). Quantification of podocalyxin labeling showed the improved vascular density using mature pre-vascularized hydrogels. Furthermore, the presence of red blood cells within the vessels labeled with the antibody specific for podocalyxin confirmed the perfusion of the implanted human engineered vessels by inosculation with the host vessels (Fig. 6G). Injection of a lectin specific for human endothelial cells further demonstrated anastomosis between the host vasculature and the implanted prevascularized network, thus providing evidence for the functionality of the microvascular network produced *in vitro* (movie 7).

We further investigated human vessels by staining collagen IV alpha 2 chain using an antibody targeting the human protein (Fig. 7A). Human vessels were lined with a strong staining of collagen IV in the basement membrane. In addition, vessels appeared as elongated and connected structures in the co-cultured pre-vascularized hydrogels, whereas round and scattered structures, sometimes lacking podocalyxin staining, were detected in the hydrogels treated with conditioned medium. We thus performed TUNEL experiments for investigation of apoptosis. Cell content of the constructs was variable both at the time of implantation, depending on seeding conditions, and at the time of sacrifice depending on invasion by host cells. We thus calculated the ratio of TUNEL stained nuclei per total nuclei inside the constructs (Fig. 7B-C). Pre-vascularization resulted in inhibition of apoptosis only when SHED were co-seeded with endothelial cells. If pre-vascularized constructs were seeded with endothelial cells only, apoptosis was similar as in control constructs, suggesting that *in vitro* maturation of capillaries was important for their integrity post-implantation. We also determined whether SHED could still undergo odontogenic/osteogenic differentiation in the tooth slice model after *in vitro* pre-vascularization. We thus performed immunolabeling for osteopontin, an early marker of the mineralization process (Fig. S6) [37]. Whatever the group, specific OPN labeling was observed with cells directly associated to the tooth slice, whereas no labeling was detected within the constructs. Finally, we also performed immunostaining for calcitonin gene related peptide (CGRP) in order to investigate innervation with sensory fibers (Fig. 7D). Quite remarkably, pre-vascularization only increased innervation when hydrogels were generated by co-culture of SHED and endothelial cells, whereas blood vessels alone had no impact, suggesting that SHED and engineered vessels had synergistic effects (Fig. 7E). Altogether, our *in vivo* data showed that *in vitro* pre-vascularization strongly enhanced blood perfusion and cell survival without altering cell differentiation and innervation, and that this effect was even stronger when mature microvascular networks were generated *in vitro*.

DISCUSSION

Rapid vascularization and establishment of a functional vascular network is a cornerstone for the clinical outcome of MSC-based therapies and pre-vascularization of tissue constructs is considered as the most promising approach to address this issue [2,3]. Whereas early studies had to deal with poor endothelial cell survival before implantation [38], we exploited the angiogenic properties of SHED that we have recently characterized [22] and demonstrated that co-culture results in effective pre-vascularization of constructs and in maturation of the microvasculature as a result of direct interactions of SHED with endothelial cells. Our study includes an original and sound methodology for quantification of MSC recruitment to vascular structures based on measurement of 3D morphometric parameters. The data thus generated demonstrate that PDGF plays a major role in SHED recruitment, resulting in acquisition of a perivascular pericyte-like phenotype and deposition of collagen IV in the vascular basement membrane. Furthermore, we show that such *in vitro* maturation of capillaries resulted in generation of a functional vascular network that improved blood perfusion and cell survival after implantation of the construct.

MSC forerunners are known to be located in the perivascular niche like pericytes [25,39], and this holds true for DPSC [27,28]. Conversely, pericytes share differentiation potency with MSC [25]. In addition, both cell types also share expression of markers of perivascular cells, including desmin, NG2 and PDGF-Rβ expressed by SHED. The emerging view of MSC as perivascular progenitor cells seems attractive and would certainly explain their isolation from virtually all vascularized organs and their pericytic phenotype [25,26,40]. The actual distinction between these two cell types is nonetheless still a matter of debate [41]. Here, most of the SHED not associated with capillaries within hydrogels displayed a star-shaped morphology and were mobile as observed by time-lapse acquisitions, both characteristics of MSC in 3D culture [30]. In contrast, SHED recruited along the vessels displayed an elongated morphology bearing membrane protrusions enwrapping the endothelium, reminiscent of pericytes [23,24]. Such a distribution along capillaries suggested that SHED play a major role in capillary stabilization. The expression of pericyte markers by MSC including SHED has however limited quantitation of their perivascular distribution [9]. We have thus developed an in-house software in order to establish morphometric parameters for quantification of perivascular cell recruitment. We have shown that PDGF-BB was responsible for SHED recruitment, as it is for pericytes *in vivo* [23], using several complementary approaches including inhibitors of its receptor PDGF-Rβ and blocking antibodies targeting PDGF. These results suggested that recruitment is based on a gradient of PDGF-BB secreted by endothelial cells and captured by heparan sulfate proteoglycans in the vicinity of capillaries [23]. In agreement with this hypothesis, we found that SHED expressed PDGF-Rβ, but that its level of expression did not correlate with recruitment. Our data rather suggested that exposure to PDGF-BB is regulating recruitment, since disrupting the PDGF-BB gradient by excess of exogenous PDGF-BB in the hydrogels inhibited recruitment. While other factors have been involved in perivascular recruitment, including TGFβ, Notch and SDF1α [23]-[42], most of these affect angiogenesis as much as perivascular cell recruitment. We performed preliminary experiments targeting CXCR4, the receptor for SDF1α that regulates pericyte and MSC perivascular recruitment [43][44][45]. The CXCR4 inhibitor AMD3100 greatly affected capillary formation together with SHED recruitment, making identification of the effects specific to perivascular recruitment quite intricate.

Pericytes regulate capillary integrity through stabilization of the basement membrane and direct interactions with endothelial cells. Indeed, whereas endothelial cells do synthesize and deposit collagen IV in the basement membrane [32,46], pericyte recruitment to capillaries further stimulates assembly of basement membrane proteins [34,47,48]. We here show that -i) the endothelial culture medium could induce collagen IV deposition by SHED, and -ii) co-culture with endothelial cells was further increasing collagen IV deposition by pericytes, suggesting mutual stimulation of synthesis and deposition of the vascular basement membrane.

Interestingly, time-lapse microscopy revealed that newly recruited SHED were quite motile along the endothelium, that could correspond to the generation of vascular guidance tunnels for perivascular cells as previously proposed [34]. Already recruited SHED displayed, however, a more stable behavior. Such a switch in behavior has already been described for MSC cultured in hydrogels functionalized with PDGF-BB in order to mimic the microenvironment of the perivascular niche [30]. The signal responsible for switching perivascular SHED behavior to a stable localization on capillaries remains, however, to be identified at the surface of capillaries. Such a signal might be associated to the generation of the basement membrane by SHED at the endothelium surface as we have shown that SHED were co-ensheathed with endothelial cells in collagen IV. A good candidate for such a switch in synthesis of extracellular matrix proteins by SHED is the Notch pathway, as recently demonstrated for other MSC using synthetic hydrogels functionalized by Jagged1, an inducer of the Notch pathway [47].

Recent studies have shown that bone marrow stromal cells have the capacity to fulfill the function of perivascular cells in regulating endothelial permeability *in vitro* [49] as pericytes [50,51]. Whereas further investigation using microfluidic devices would be necessary for characterizing the functional consequences of vascular maturation by SHED, we here investigated the functional impact post-implantation of microvascular prior maturation. As expected, we first showed that implantation of *in vitro* pre-vascularized constructs strongly improved blood perfusion, using both Micro-CT dynamic acquisition and vWF immunostaining. Such results are consistent with those obtained using different approaches for *in vitro* pre-vascularization including hydrogels [52,53], spheroids [8] or cell sheets [54]. Using SHED conditioned medium, we could also generate microvascular networks composed of endothelial cells alone and devoid of perivascular cell-mediated maturation. This tool allowed us to assess the importance of *in vitro* maturation on post-implantation vascularization of the constructs. Indeed, using human specific antibodies, we demonstrated that *in vitro* maturation further improved *in vivo* vascularization with better vascular morphology and basement membrane deposition by the human capillaries, as well as protection from apoptosis in the constructs. It should be noted that such maturation of capillaries occurred rapidly and at the mm^3 scale, as 4 days in co-culture were sufficient for improved cell survival in the construct. Furthermore, maturation of the whole hydrogel as a result of micro-environment remodeling by SHED could participate to the improved vascularization that we observed, even though such effects have been described using smaller microgels and after much longer *in vitro* pre-culture (14 days in culture) [55]. Gel contraction *in vivo* prevented comparison of vascular densities before and after implantation, and thus prevented assessment of the growth or loss of implanted human vessels. In addition, we could not detect significant differences in capillary densities using antibodies targeting either human only or human and mouse endothelial cells. We measured, however, a much higher level of apoptosis in constructs seeded with endothelial cells alone, suggesting that the difference in vascular density was

more probably resulting from loss of implanted vessels than from post-implantation expansion of the microvasculature in gels co-seeded with endothelial cells and SHED. Altogether, these data suggested that perfusion of the construct mostly relied on the human vessels engineered *in vitro*.

Finally, engineered vessels were surrounded by sensory nerve fibers, notably in the EC-SHED group. These sensory fibers are important for the future functionality of the implanted engineered tissue [56]. Remarkably, no osteopontin expression was detected at proximity of the implanted vessels, confirming the absence of osteogenic differentiation of SHED in the vessel vicinity. In contrast, several cells adjacent to the tooth section were osteopontin positive, suggesting that, despite the treatments to which cells were exposed during the pre-vascularization process, some were still able to undergo odontogenic/osteogenic differentiation when placed in an odontogenic environment [57], as previously reported [22]-[36]. In the future, functional assays such as tissue injury model will have to be conducted to demonstrate the functionality of the engineered implanted tissue.

CONCLUSION

Altogether, this study demonstrates the interest of SHED in a pre-vascularization strategy for tissue engineering. These cells have the capacity to directly participate in the vessel maturation by displaying a pericyte-like morphology and by its reinforcement through basement membrane deposition. This interaction allows better perfusion and survival of the engineered vascular network upon implantation, supporting the rapid establishment of a functional vascular network within the implanted construct and therefore a favorable outcome of the graft in a clinical perspective. These results introduce important clinical prospects that should improve success of cell-based therapies for which promoting cell survival and improving blood perfusion remains the major challenge. Further studies in large animal models using autologous cells are now needed to confirm the clinical relevance of this strategy. In parallel with these applications, the functional validation that inosculation demonstrates in our study supports the use of such pre-vascularized hydrogels as tools for *in vitro* investigation of angiogenesis and vascular integrity in 3D settings.

MATERIALS AND METHODS

Cell culture

Culture of human dental pulp stem cells from exfoliated deciduous teeth (SHEDs) was established as previously reported [58]. Deciduous teeth were collected after trauma or after exfoliation from three healthy young children (3-7 years of age). Briefly, after decontamination with povidone-iodine solution (Betadine, Meda Pharma, France), teeth were sectioned longitudinally and exposed pulp tissues were collected and enzymatically digested with type I collagenase (3 mg/ml; Worthington Biochem, Freehold, NJ, USA) and dispase (2 U/ml; Roche, Mannheim, Germany). Cells were then cultured in Modified Eagle Medium alpha (alphaMEM; Invitrogen, Grand island, NY, USA) supplemented with 20% fetal bovine serum (FBS; Invitrogen), 1% penicillin/streptomycin (Invitrogen), at 37°C with 5% CO_2. The medium was refreshed after 3 days and then twice a week. Cells were detached by trypsinization at 70% confluence (0.25% trypsin EDTA solution Sigma-Aldrich, St. Louis, MO) and either frozen at -80 °C or re-plated at a density of 10^4 cells/cm^2 in Dulbecco's Modified Eagle Medium 1g/L D-Glucose (DMEM low glucose; Invitrogen, Grand island, NY) supplemented with 10% fetal bovine serum (FBS; Invitrogen), 1% penicillin/streptomycin (Invitrogen), at 37°C with 5% CO_2 with medium refreshing twice a week. For all experiments, SHEDs were used between passages 2 and 5.

Human endothelial cells from the umbilical vein were prepared as previously described [59]. They were cultivated on type I collagen (100 µg/mL) in endothelial cell growth medium 2 (ECGM2, PromoCell, Heidelberg, Germany). Experiments were performed before passage 5. Adult normal human dermal fibroblasts (NHDF, Promocell, Heidelberg, Germany) and Vascular Smooth Muscle cells (vSMC,) were grown in fibroblast growth medium 2 (FGM2; PromoCell). Human pericytes from placenta (gift from B. Péault, MRC Center for Regenerative Medicine, University of Edinburgh) were cultured in DMEM Low Glucose (Gibco, Hampton, US) supplemented with 20% FBS.

For some experiments SHED and endothelial cells were transfected with a LifeAct-Ruby lentivirus or a pSico GFP lentivirus respectively.

In vitro vascularization and tissue construct preparation

Endothelial cells were either seeded alone or co-seeded with SHED at the indicated concentrations in 2 mg/ml collagen I extracted from rat tail. Hydrogels were cast either in Ibidi µ-insert for observation on the DSLM or in tooth slice for *in vivo* implantation. In order to promote adhesion of the hydrogel to the scaffold, µ-inserts were coated with 1.5 mg/ml poly-dopamine (Sigma-Aldrich) in 10 mM tris pH8.5 overnight in the dark. Tooth slices (one slice per well) were placed into 24-well cell culture-suspension plates (Cellstar, Greiner bio-one, Basel, Switzerland). For implantation experiments, control gels only contained SHED cells at 1 x 10^6 cells/ml. Hydrogels were cultured for 3 or 4 days either in SHED conditioned medium or in ECGM2 depleted for VEGF.

Capillary formation and perivascular cell recruitment were analyzed using the Cytodex bead assay [31,32]. Endothelial cells were seeded on Cytodex beads (GE Healthcare, Knoxville, TN) 24 hours before embedding in a 2.5 mg/mL fibrin gel containing SHED at 1 x 10^6 cells/ml. Gels were then incubated in ECGM2 depleted for VEGF. Inhibitors (Imatinib mesylate® R&D Systems, 5906/100), blocking antibody (anti-PDGF, R&D Systems, AB-23-NA), recombinant protein (rhPDGF-BB, R&D Systems, 220-BB-010) or heparin (Promocell, C-39211) were added at the indicated concentrations in the culture medium.

Immunofluorescence

2D and 3D samples were fixed with 4% paraformaldehyde for 10 min and 30 min respectively, permeabilized with 0.5% triton-X-100 (Sigma-Aldrich) and saturated only for 2D culture with 10% normal goat serum. They were then incubated with primary antibodies directed against CD31 (1/200, Dako, Les Ulis, France, M0823), Col IV α2 chain (1/400, Sigma-Aldrich, MAB1910), αSMA coupled to Dylight550 (1/100, Novus, NBP2-44464R), Desmin (1/200, Molecular Probes, Molecular Probes, 131-15015), PDGF-β receptor coupled to Alexa Fluor647 (1/100, Abcam, ab196151), NG2 (1/200, Abcam, ab5320). They were then incubated with secondary antibodies targeting mouse IgG coupled to Alexa555 or goat IgG coupled to Alexa488 (1/500, Invitrogen). Actin was stained with Phalloidin coupled to complementary AlexaFluor (1/200, Invitrogen). Nuclei were stained with 4',6-diamidino-2-phenylindole (DAPI) (1/10000, Invitrogen).

Image acquisition and quantification

Analysis of 2D immunostaining was performed with a Zeiss Observer Apotome 2 using Plan-Apochromat 63x/1.4 oil-immersion objective lens. For capillary network acquisition, images were acquired using Plan-Apochromat 10x/0.45 or 20x/0.8 objective lens or with in-house DSLM. Time-lapse acquisitions have also been performed with the DSLM (supplementary material and methods for detailed description). For capillary network quantification, images were segmented to obtain a 3D mask and further analyzed with in-house software (3D-Skel, Fig. S1) developed on Matlab (Matworks) using Skel2Graph3D [60]. MIJ pluging (http://bigwww.epfl.ch/sage/soft/mij/) was used to interact with ImageJ (NIH, Bethesda MD, USA) (http://www.imagej.nih.gov/ij) in order to create and analyze the parameters of the 3D vessel skeleton [61]. Quantification of perivascular cell recruitment was based on the 3D measurement of the distance between SHED nuclei and capillary surface stained with CD31 and converted into 3D surface. SHED nuclei were isolated by image processing with the Imaris Xtension module "Distance Transformation" and converted into spots. Those, outside capillary surfaces, were sorted for automatic 3D distance measurement. Threshold was adjusted to allow automatic detection and quantification of perivascular recruitment.

Human tooth slice preparation

Teeth were obtained from the Dental Departments of AP-HP, France. For tooth section preparation, permanent third molars were obtained in young adults (18-25 years of age) after extraction according to an orthodontic treatment plan. All teeth were collected with informed and oral consent from the patients and the parents according to ethical guidelines set by the French law and with a dedicated authorization for UR246 (n°DC-2009-927, Cellule Bioéthique DGRI/A5, Paris, France).

One-mm-thick tooth slices were prepared from caries-free third molars as previously described [22,62,63]. After disinfection with 70% ethanol, teeth were transversely sectioned at the cervical region using a diamond saw blade under cooling with sterile phosphate-buffered saline (PBS, Invitrogen) to obtain 1-mm-thick dentin slices. The pulp tissue was completely removed and tooth slices were immersed in 0.05% sodium hypochlorite for 10 s and then washed with sterile PBS.

Ethical approval and animal management

All experiments in this study were designed according to ARRIVE guidelines and performed according to protocols approved by the Animal Care Committee of University Paris Descartes (APAFIS #6173). Animals were maintained according to the guidelines for ethical conduct developed by the European Communities Council Directive (animal breeding agreement D92-049-01). All efforts were made to minimize their pain or discomfort. Athymic NUDE "NMRI-Foxn1 nu/nu" male mice (6 weeks – old, ≈30g) were purchased from Janvier Labs (Le Genest Saint Isle, France). They were housed at sterile stable conditions (22±2 ºC) with a 12h dark/light cycle, and with ad libitum access to sterilized water and food.

Surgical procedure

Tissue constructs were implanted in Athymic Nude mice (n=15 per group) as described [22]. During the entire surgery procedure, the animals were maintained in a sterile environment using a laminar flow hood Esolis 1200 Noroit®. Analgesia injection with buprenorphine (0.02 mg/kg b.w.) was performed 15 minutes before surgery to prevent pain. Athymic NUDE mice were anesthetized with 80mg/kg b.w. of ketamine and 10mg/kg b.w. of xylazine hydrochloride, both from Centravet (Maison-Alfort, France). Two tissue constructs kept in serum-free medium were implanted subcutaneously in each side of the mouse back (Agreement CEE A34.CC.003.11). Each animal was randomly allocated *per* cage and *per* group. Wound closure was achieved by suturing the skin using absorbable suture (Vicryl Rapid 4.0, Ethicon, Johnson & Jonhson). Wound healing progressed without any sign of infection, material exposure or other complication.

Micro-X-ray computed tomography (Micro-CT) analysis

For exploration of angiogenesis in tissue constructs, mice were anesthetized and an intracardiac (left ventricle) injection of a contrast agent (Barium sulfate dilute in PBS) was performed before scanning using an X-ray micro-CT device (Quantum FX Caliper, Life Sciences, Perkin Elmer, Waltham, MA) hosted by the IDV Platform, UR2496, Montrouge, France. The X-ray source was set at 90 kV and 160 µA. Tridimensional images were acquired with an isotropic voxel size of 20 µm. Full 3D high-resolution raw data are obtained by rotating both the X-ray source and the flat panel detector 360° around the sample (scanning time: 3 min). After acquiring the 360° projections, the 3D reconstructions were obtained using RigakuSW (Caliper) software (a voxels matrix of 512x512x512 with 20 µm of resolution). Tridimensional rendering was subsequently extracted from Dicom data frames using the open-source OsiriX imaging software (v3.7.1, distributed under LGPL license, Dr A. Rosset, Geneva, Switzerland). Quantification of the vascular density inside each tissue construct was realized using Analyse 11.0 (Biomedical Imaging Resource, Mayo Clinic, Rochester, MN, USA). A global volume of interest (VOI) was drawn by interpolating 2D region of interests on consecutive sections to isolate tissue constructs. The obtained interpolated VOI comprised only 3D collagen matrices and the invading vessels into which lumens were counter-contrasted using barium chloride. To reduce the background noise, we used spatial filter (median 3x3x3). Vessels were finally segmented with a threshold, that selected barium chloride-contrasted vessels in Volume Edit, and vascular volume fraction (%) was calculated with region of interest in Analyze 11.0.

Immunohistochemistry and immunofluorescence

Thirty days after *in vivo* implantation, tissue constructs were surgically removed and fixed

overnight at 4°C in 4% paraformaldehyde, then progressively demineralized in 4.13% pH 7.3 EDTA (n=15 tissue constructs per group). Tissues were embedded in paraffin and 7 µm sections were prepared for immunohistochemistry. Samples were deparaffinized, and non-specific peroxidases were blocked for 15 min with ortho-periodic acid. Non-specific protein binding was blocked with 5% BSA during 1 hour after treated with 0.1% PronaseE during 10 min at 35°C. Samples were incubated overnight at 4°C, with primary antibody: vWF (1/800; ab6994, Abcam, Cambridge, UK), and Osteopontin (1/100; AF1433, R&D system, Minneapolis, Minnesota, USA). Samples were rinsed and incubated with polyclonal anti-rabbit or anti-goat immunoglobulin (1/1000, Dako, Glostrup, Denmark). Color reaction was developed with 3.30- Diaminobenzidine tetrahydrochloride (Fast Dab, Sigma-Aldrich), and samples were counterstained with eosin and hematoxylin (Vector). Double-labelling immunofluorescence were performed by consecutively treating the sections with antibodies targeting human podocalyxin (1/20, AF1658, R&D system, Minneapolis, Minnesota, USA) and Coll IV a3 (1/100, Novotech 20411, Bron, France) and fluorescent-labelled secondary antibodies (Goat Alexa 555 and Rabbit Alexa 647, respectively) diluted at 1/200 and 1/100, respectively. Nuclei were stained with 4',6-diamidino-2-phenylindole (DAPI) (Invitrogen). Sensitive fibers immunofluorescence was performed using a CGRP polyclonal antibody (1/500; C8198, Sigma-Aldrich, Saint Louis, Missouri, USA) and a fluorescent-labelled secondary goat anti-rabbit antibody (Rhodamine Red-X at 1/100, Thermofisher, Waltham, MA USA). Negative controls were included by the omission of primary antibodies. Apoptosis was evaluated by the TUNEL reaction (In situ cell death detection fluorescein Roche 11,684,795,910). To quantify vascularization and apoptosis, sections were observed with a microscope equipped with 10X and 20X objectives, respectively (Leica Microsystems Wetzlar GmbH). Area of vascularization and number of apoptotic nuclei were measured using ImageJ software. Slices were chosen to be spaced throughout tissue constructs to quantify vascularization area in full lengthwise and apoptosis in representative areas.

Statistical Analysis

Numerical variables are expressed as the mean ± standard deviation (SD). The statistical analyses were performed using Prism software version 7.04 (GraphPad software, Paris Descartes). The normality of the distribution was tested with the D'Agostino-Pearson Normality test and Shapiro Wilks Normality test. The homogeneity of variance was tested with the Fisher *F* test. When the distribution of the data for each group respected the normality law and the variance of the group was homogeneous, the *t* test for independent measures was used to compare two group means. When the distribution of at least one of the groups did not follow the normality law or is too small to be tested, comparison between groups were performed with the nonparametric Kruskal-Wallis test, followed by group comparison with the Mann-Whitney *U* test. To compare the 3 groups at each time-point a one-way Anova was performed followed by a Bonferroni test. For animal experiments, the tooth slice was considered as the statistical unit. Differences were considered significant at $p<0.05$.

FUNDING

Experiments and building of the light-sheet microscope were supported by grants from Fondation pour la Recherche Médicale (DBS20131128438) and ANR PulpCell to CC and LM, and from Fondation des Gueules Cassées to UR2496. Micro-CT device was funded by Fondation pour la Recherche Médicale for Plateforme d'imagerie du Vivant Paris Descartes and UR2496 (FRM DGE20111123012). YA was supported by la Ligue Nationale contre le Cancer, AN by Ministère de l'Enseignement Supérieur et de la Recherche and MFM and EC by Fondation pour la Recherche Médicale.

ACKNOWLEDGEMENTS

Authors thank Pr Cécile Badoual (Université de Paris, PARCC, Inserm, Paris, France) for helpful discussion regarding CGRP quantification.

AUTHOR CONTRIBUTIONS

Yoann Atlas: Conceptualization, Methodology, Software, Formal analysis, Investigation, Visualization, Writing- Original draft preparation. **Caroline Gorin**: Conceptualization, Formal analysis, Investigation, Visualization, Writing- Original draft preparation. **Anita Novais**: Investigation, Visualization. **Julie Lesieur, Clément Binet-Moussy, Eirini Chatzopoulou, Marion Marchand, Rumeyza Bascetin, Jeremy Sadoine, Matthieu Lesage** : Investigation. **Sybille Opsal-Vital**: Resources, Writing-Reviewing and Editing. **Bruno M Péault**: Resources, Writing-Reviewing and Editing. **Catherine Monnot**: Conceptualization, Writing-Reviewing and Editing. **Anne Polliard**: Writing-Reviewing and Editing. **Philippe Girard**: Methodology, Software, Writing-Reviewing and Editing. **Stephane Germain**: Conceptualization, Writing-Reviewing and Editing, Funding Acquisition. **Catherine Chaussain and Laurent Muller**: Conceptualization, Supervision, and Writing- Original draft preparation, Funding Acquisition

DECLARATION OF INTERESTS

The authors declare that they have no known competing financial interests or personal relationships that could have appeared to influence the work reported in this paper.

DATA AVAILABILITY

The raw/processed data required to reproduce these findings cannot be shared at this time due to technical or time limitations.

REFERENCES

[1] E.C. Novosel, C. Kleinhans, P.J. Kluger, Vascularization is the key challenge in tissue engineering, Adv. Drug Deliv. Rev. 63 (2011) 300–311. https://doi.org/10.1016/j.addr.2011.03.004.

[2] H.-H. Greco Song, R.T. Rumma, C.K. Ozaki, E.R. Edelman, C.S. Chen, Vascular Tissue Engineering: Progress, Challenges, and Clinical Promise, Cell Stem Cell. 22 (2018) 608. https://doi.org/10.1016/j.stem.2018.03.014.

[3] T. Rademakers, J.M. Horvath, C.A. van Blitterswijk, V.L.S. LaPointe, Oxygen and nutrient delivery in tissue engineering: Approaches to graft vascularization, J Tissue Eng Regen Med. 13 (2019) 1815–1829. https://doi.org/10.1002/term.2932.

[4] X. Chen, A.S. Aledia, S.A. Popson, L. Him, C.C.W. Hughes, S.C. George, Rapid anastomosis of endothelial progenitor cell-derived vessels with host vasculature is promoted by a high density of cotransplanted fibroblasts, Tissue Eng Part A. 16 (2010) 585–594. https://doi.org/10.1089/ten.TEA.2009.0491.

[5] G. Cheng, S. Liao, H. Kit Wong, D.A. Lacorre, E. di Tomaso, P. Au, D. Fukumura, R.K. Jain, L.L. Munn, Engineered blood vessel networks connect to host vasculature via wrapping-and-tapping anastomosis, Blood. 118 (2011) 4740–4749. https://doi.org/10.1182/blood-2011-02-338426.

[6] D. Marino, J. Luginbühl, S. Scola, M. Meuli, E. Reichmann, Bioengineering dermo-epidermal skin grafts with blood and lymphatic capillaries, Sci Transl Med. 6 (2014) 221ra14. https://doi.org/10.1126/scitranslmed.3006894.

[7] S.B. Riemenschneider, D.J. Mattia, J.S. Wendel, J.A. Schaefer, L. Ye, P.A. Guzman, R.T. Tranquillo, Inosculation and perfusion of pre-vascularized tissue patches containing aligned human microvessels after myocardial infarction, Biomaterials. 97 (2016) 51–61. https://doi.org/10.1016/j.biomaterials.2016.04.031.

[8] C. Mazio, C. Casale, G. Imparato, F. Urciuolo, C. Attanasio, M. De Gregorio, F. Rescigno, P.A. Netti, Pre-vascularized dermis model for fast and functional anastomosis with host vasculature, Biomaterials. 192 (2019) 159–170. https://doi.org/10.1016/j.biomaterials.2018.11.018.

[9] U. Blache, M. Ehrbar, Inspired by Nature: Hydrogels as Versatile Tools for Vascular Engineering, Adv Wound Care (New Rochelle). 7 (2018) 232–246. https://doi.org/10.1089/wound.2017.0760.

[10] M. Marchand, C. Monnot, L. Muller, S. Germain, Extracellular matrix scaffolding in angiogenesis and capillary homeostasis, Semin. Cell Dev. Biol. 89 (2019) 147–156. https://doi.org/10.1016/j.semcdb.2018.08.007.

[11] A. Sorushanova, L.M. Delgado, Z. Wu, N. Shologu, A. Kshirsagar, R. Raghunath, A.M. Mullen, Y. Bayon, A. Pandit, M. Raghunath, D.I. Zeugolis, The Collagen Suprafamily: From Biosynthesis to Advanced Biomaterial Development, Adv. Mater. Weinheim. 31 (2019) e1801651. https://doi.org/10.1002/adma.201801651.

[12] M. Potente, T. Mäkinen, Vascular heterogeneity and specialization in development and disease, Nat. Rev. Mol. Cell Biol. 18 (2017) 477–494. https://doi.org/10.1038/nrm.2017.36.

[13] S. Gronthos, M. Mankani, J. Brahim, P.G. Robey, S. Shi, Postnatal human dental pulp stem cells (DPSCs) in vitro and in vivo, Proc. Natl. Acad. Sci. U.S.A. 97 (2000) 13625–13630. https://doi.org/10.1073/pnas.240309797.

[14] M. La Noce, F. Paino, A. Spina, P. Naddeo, R. Montella, V. Desiderio, A. De Rosa, G. Papaccio, V. Tirino, L. Laino, Dental pulp stem cells: state of the art and suggestions for a true translation of research into therapy, J Dent. 42 (2014) 761–768. https://doi.org/10.1016/j.jdent.2014.02.018.

[15] P. Hilkens, N. Meschi, P. Lambrechts, A. Bronckaers, I. Lambrichts, Dental Stem Cells in Pulp Regeneration: Near Future or Long Road Ahead?, Stem Cells Dev. 24 (2015) 1610–1622. https://doi.org/10.1089/scd.2014.0510.

[16] Y. Yamada, S. Nakamura-Yamada, K. Kusano, S. Baba, Clinical Potential and Current Progress of Dental Pulp Stem Cells for Various Systemic Diseases in Regenerative Medicine: A Concise Review, International Journal of Molecular Sciences. 20 (2019) 1132. https://doi.org/10.3390/ijms20051132.

[17] M. Nakashima, K. Iohara, M. Murakami, H. Nakamura, Y. Sato, Y. Ariji, K. Matsushita, Pulp regeneration by transplantation of dental pulp stem cells in pulpitis: a pilot clinical study, Stem Cell Res Ther. 8 (2017) 1–13. https://doi.org/10.1186/s13287-017-0506-5.

[18] M. Nakashima, K. Iohara, Recent Progress in Translation from Bench to a Pilot Clinical Study on Total Pulp Regeneration, Journal of Endodontics. 43 (2017) S82–S86. https://doi.org/10.1016/j.joen.2017.06.014.

[19] K. Xuan, B. Li, H. Guo, W. Sun, X. Kou, X. He, Y. Zhang, J. Sun, A. Liu, L. Liao, S. Liu, W. Liu, C. Hu, S. Shi, Y. Jin, Deciduous autologous tooth stem cells regenerate dental pulp after implantation into injured teeth, Science Translational Medicine. 10 (2018). https://doi.org/10.1126/scitranslmed.aaf3227.

[20] A. Bronckaers, P. Hilkens, Y. Fanton, T. Struys, P. Gervois, C. Politis, W. Martens, I. Lambrichts, Angiogenic properties of human dental pulp stem cells, PLoS ONE. 8 (2013) e71104. https://doi.org/10.1371/journal.pone.0071104.

[21] W.L. Dissanayaka, L. Zhu, K.M. Hargreaves, L. Jin, C. Zhang, In vitro analysis of scaffold-free prevascularized microtissue spheroids containing human dental pulp cells and endothelial cells, J Endod. 41 (2015) 663–670. https://doi.org/10.1016/j.joen.2014.12.017.

[22] C. Gorin, G.Y. Rochefort, R. Bascetin, H. Ying, J. Lesieur, J. Sadoine, N. Beckouche, S. Berndt, A. Novais, M. Lesage, B. Hosten, L. Vercellino, P. Merlet, D. Le-Denmat, C. Marchiol, D. Letourneur, A. Nicoletti, S.O. Vital, A. Poliard, B. Salmon, L. Muller, C. Chaussain, S. Germain, Priming Dental Pulp Stem Cells With Fibroblast Growth Factor-2 Increases Angiogenesis of Implanted Tissue-Engineered Constructs Through Hepatocyte Growth Factor and Vascular Endothelial Growth Factor Secretion, Stem Cells Transl Med. 5 (2016) 392–404. https://doi.org/10.5966/sctm.2015-0166.

[23] A. Armulik, G. Genové, C. Betsholtz, Pericytes: developmental, physiological, and pathological perspectives, problems, and promises, Dev. Cell. 21 (2011) 193–215. https://doi.org/10.1016/j.devcel.2011.07.001.

[24] E.M. Shen, K.E. McCloskey, Development of Mural Cells: From In Vivo Understanding to In Vitro Recapitulation, Stem Cells Dev. 26 (2017) 1020–1041. https://doi.org/10.1089/scd.2017.0020.

[25] M. Crisan, S. Yap, L. Casteilla, C.-W. Chen, M. Corselli, T.S. Park, G. Andriolo, B. Sun, B. Zheng, L. Zhang, C. Norotte, P.-N. Teng, J. Traas, R. Schugar, B.M. Deasy, S. Badylak, H.-J. Buhring, J.-P. Giacobino, L. Lazzari, J. Huard, B. Péault, A perivascular origin for mesenchymal stem cells in multiple human organs, Cell Stem Cell. 3 (2008) 301–313. https://doi.org/10.1016/j.stem.2008.07.003.

[26] L.E.B. de Souza, T.M. Malta, S. Kashima Haddad, D.T. Covas, Mesenchymal Stem Cells and Pericytes: To What Extent Are They Related?, Stem Cells Dev. 25 (2016) 1843–1852. https://doi.org/10.1089/scd.2016.0109.

[27] S. Shi, S. Gronthos, Perivascular niche of postnatal mesenchymal stem cells in human bone marrow and dental pulp, J. Bone Miner. Res. 18 (2003) 696–704. https://doi.org/10.1359/jbmr.2003.18.4.696.

[28] K. Janebodin, Y. Zeng, W. Buranaphatthana, N. Ieronimakis, M. Reyes, VEGFR2-dependent angiogenic capacity of pericyte-like dental pulp stem cells, J. Dent. Res. 92 (2013) 524–531. https://doi.org/10.1177/0022034513485599.

[29] M. Ducret, H. Fabre, O. Degoul, G. Atzeni, C. McGuckin, N. Forraz, F. Mallein-Gerin, E. Perrier-Groult, B. Alliot-Licht, J.-C. Farges, Immunophenotyping Reveals the Diversity of Human Dental Pulp Mesenchymal Stromal Cells In vivo and Their Evolution upon In vitro Amplification, Front Physiol. 7 (2016) 512. https://doi.org/10.3389/fphys.2016.00512.

[30] P.S. Lienemann, Y.R. Devaud, R. Reuten, B.R. Simona, M. Karlsson, W. Weber, M. Koch, M.P. Lutolf, V. Milleret, M. Ehrbar, Locally controlling mesenchymal stem cell morphogenesis by 3D PDGF-BB gradients towards the establishment of an in vitro perivascular niche, Integr Biol (Camb). 7 (2015) 101–111. https://doi.org/10.1039/c4ib00152d.

[31] M.N. Nakatsu, C.C.W. Hughes, An optimized three-dimensional in vitro model for the analysis of angiogenesis, Meth. Enzymol. 443 (2008) 65–82. https://doi.org/10.1016/S0076-6879(08)02004-1.

[32] M. Bignon, C. Pichol-Thievend, J. Hardouin, M. Malbouyres, N. Bréchot, L. Nasciutti, A. Barret, J. Teillon, E. Guillon, E. Etienne, M. Caron, R. Joubert-Caron, C. Monnot, F. Ruggiero, L. Muller, S. Germain, Lysyl oxidase-like protein-2 regulates sprouting angiogenesis and type IV collagen assembly in the endothelial basement membrane, Blood. 118 (2011) 3979–3989. https://doi.org/10.1182/blood-2010-10-313296.

[33] A. Abramsson, S. Kurup, M. Busse, S. Yamada, P. Lindblom, E. Schallmeiner, D. Stenzel, D. Sauvaget, J. Ledin, M. Ringvall, U. Landegren, L. Kjellén, G. Bondjers, J. Li, U. Lindahl, D. Spillmann, C. Betsholtz, H. Gerhardt, Defective N-sulfation of heparan sulfate proteoglycans limits PDGF-BB binding and

pericyte recruitment in vascular development, Genes Dev. 21 (2007) 316–331. https://doi.org/10.1101/gad.398207.

[34] A.N. Stratman, K.M. Malotte, R.D. Mahan, M.J. Davis, G.E. Davis, Pericyte recruitment during vasculogenic tube assembly stimulates endothelial basement membrane matrix formation, Blood. 114 (2009) 5091–5101. https://doi.org/10.1182/blood-2009-05-222364.

[35] R. Jayadev, D.R. Sherwood, Basement membranes, Curr Biol. 27 (2017) R207–R211. https://doi.org/10.1016/j.cub.2017.02.006.

[36] F.F. Demarco, L. Casagrande, Z. Zhang, Z. Dong, S.B. Tarquinio, B.D. Zeitlin, S. Shi, A.J. Smith, J.E. Nör, Effects of Morphogen and Scaffold Porogen on the Differentiation of Dental Pulp Stem Cells, Journal of Endodontics. 36 (2010) 1805–1811. https://doi.org/10.1016/j.joen.2010.08.031.

[37] J. Sodek, B. Ganss, M.D. McKee, Osteopontin, Crit. Rev. Oral Biol. Med. 11 (2000) 279–303. https://doi.org/10.1177/10454411000110030101.

[38] J.S. Schechner, A.K. Nath, L. Zheng, M.S. Kluger, C.C. Hughes, M.R. Sierra-Honigmann, M.I. Lorber, G. Tellides, M. Kashgarian, A.L. Bothwell, J.S. Pober, In vivo formation of complex microvessels lined by human endothelial cells in an immunodeficient mouse, Proc. Natl. Acad. Sci. U.S.A. 97 (2000) 9191–9196. https://doi.org/10.1073/pnas.150242297.

[39] M.F. Pittenger, D.E. Discher, B.M. Péault, D.G. Phinney, J.M. Hare, A.I. Caplan, Mesenchymal stem cell perspective: cell biology to clinical progress, Npj Regen Med. 4 (2019) 22. https://doi.org/10.1038/s41536-019-0083-6.

[40] A.W. James, B. Péault, Perivascular Mesenchymal Progenitors for Bone Regeneration, J. Orthop. Res. 37 (2019) 1221–1228. https://doi.org/10.1002/jor.24284.

[41] V. Yianni, P.T. Sharpe, Perivascular-Derived Mesenchymal Stem Cells, J. Dent. Res. 98 (2019) 1066–1072. https://doi.org/10.1177/0022034519862258.

[42] C.R. Harrell, B.S. Markovic, C. Fellabaum, A. Arsenijevic, V. Djonov, V. Volarevic, Molecular mechanisms underlying therapeutic potential of pericytes, J Biomed Sci. 25 (2018) 1–12. https://doi.org/10.1186/s12929-018-0423-7.

[43] N. Song, Y. Huang, H. Shi, S. Yuan, Y. Ding, X. Song, Y. Fu, Y. Luo, Overexpression of Platelet-Derived Growth Factor-BB Increases Tumor Pericyte Content via Stromal-Derived Factor-1α/CXCR4 Axis, Cancer Res. 69 (2009) 6057–6064. https://doi.org/10.1158/0008-5472.CAN-08-2007.

[44] A.N. Stratman, M.J. Davis, G.E. Davis, VEGF and FGF prime vascular tube morphogenesis and sprouting directed by hematopoietic stem cell cytokines, Blood. 117 (2011) 3709–3719. https://doi.org/10.1182/blood-2010-11-316752.

[45] L. Cheng, Z. Huang, W. Zhou, Q. Wu, S. Donnola, J.K. Liu, X. Fang, A.E. Sloan, Y. Mao, J.D. Lathia, W. Min, R.E. McLendon, J.N. Rich, S. Bao, Glioblastoma Stem Cells Generate Vascular Pericytes to Support Vessel Function and Tumor Growth, Cell. 153 (2013) 139–152. https://doi.org/10.1016/j.cell.2013.02.021.

[46] R.C.A. Sainson, J. Aoto, M.N. Nakatsu, M. Holderfield, E. Conn, E. Koller, C.C.W. Hughes, Cell-autonomous notch signaling regulates endothelial cell branching and proliferation during vascular tubulogenesis, FASEB J. 19 (2005) 1027–1029. https://doi.org/10.1096/fj.04-3172fje.

[47] U. Blache, Q. Vallmajo-Martin, E.R. Horton, J. Guerrero, V. Djonov, A. Scherberich, J.T. Erler, I. Martin, J.G. Snedeker, V. Milleret, M. Ehrbar, Notch-inducing hydrogels reveal a perivascular switch of mesenchymal stem cell fate, EMBO Rep. 19 (2018). https://doi.org/10.15252/embr.201845964.

[48] Z. Zhou, F. Pausch, U. Schlötzer-Schrehardt, B. Brachvogel, E. Pöschl, Induction of initial steps of angiogenic differentiation and maturation of endothelial cells by pericytes in vitro and the role of collagen IV, Histochem. Cell Biol. 145 (2016) 511–525. https://doi.org/10.1007/s00418-015-1398-z.

[49] S. Alimperti, T. Mirabella, V. Bajaj, W. Polacheck, D.M. Pirone, J. Duffield, J. Eyckmans, R.K. Assoian, C.S. Chen, Three-dimensional biomimetic vascular model reveals a RhoA, Rac1, and N-cadherin balance in mural cell-endothelial cell-regulated barrier function, Proc. Natl. Acad. Sci. U.S.A. 114 (2017) 8758–8763. https://doi.org/10.1073/pnas.1618333114.

[50] J. Kim, M. Chung, S. Kim, D.H. Jo, J.H. Kim, N.L. Jeon, Engineering of a Biomimetic Pericyte-Covered 3D Microvascular Network, PLoS ONE. 10 (2015) e0133880. https://doi.org/10.1371/journal.pone.0133880.

[51] M. Campisi, Y. Shin, T. Osaki, C. Hajal, V. Chiono, R.D. Kamm, 3D self-organized microvascular model of the human blood-brain barrier with endothelial cells, pericytes and astrocytes, Biomaterials. 180 (2018) 117–129. https://doi.org/10.1016/j.biomaterials.2018.07.014.

[52] X. Chen, A.S. Aledia, C.M. Ghajar, C.K. Griffith, A.J. Putnam, C.C.W. Hughes, S.C. George, Prevascularization of a fibrin-based tissue construct accelerates the formation of functional anastomosis with host vasculature, Tissue Eng Part A. 15 (2009) 1363–1371. https://doi.org/10.1089/ten.tea.2008.0314.

[53] S. Ben-Shaul, S. Landau, U. Merdler, S. Levenberg, Mature vessel networks in engineered tissue promote graft-host anastomosis and prevent graft thrombosis, Proc. Natl. Acad. Sci. U.S.A. 116 (2019) 2955–2960. https://doi.org/10.1073/pnas.1814238116.

[54] L. Gibot, T. Galbraith, J. Huot, F.A. Auger, A preexisting microvascular network benefits in vivo revascularization of a microvascularized tissue-engineered skin substitute, Tissue Eng Part A. 16 (2010) 3199–3206. https://doi.org/10.1089/ten.tea.2010.0189.

[55] A.L. Torres, S.J. Bidarra, D.P. Vasconcelos, J.N. Barbosa, E.A. Silva, D.S. Nascimento, C.C. Barrias, Microvascular engineering: Dynamic changes in microgel-entrapped vascular cells correlates with higher vasculogenic/angiogenic potential, Biomaterials. 228 (2020) 119554. https://doi.org/10.1016/j.biomaterials.2019.119554.

[56] W. Martens, K. Sanen, M. Georgiou, T. Struys, A. Bronckaers, M. Ameloot, J. Phillips, I. Lambrichts, Human dental pulp stem cells can differentiate into Schwann cells and promote and guide neurite outgrowth in an aligned tissue-engineered collagen construct in vitro, FASEB J. 28 (2014) 1634–1643. https://doi.org/10.1096/fj.13-243980.

[57] R.N. D'Souza, A.L. Bronckers, R.P. Happonen, D.A. Doga, M.C. Farach-Carson, W.T. Butler, Developmental expression of a 53 KD dentin sialoprotein in rat tooth organs, J. Histochem. Cytochem. 40 (1992) 359–366. https://doi.org/10.1177/40.3.1552175.

[58] M. Miura, S. Gronthos, M. Zhao, B. Lu, L.W. Fisher, P.G. Robey, S. Shi, SHED: stem cells from human exfoliated deciduous teeth, Proc. Natl. Acad. Sci. U.S.A. 100 (2003) 5807–5812. https://doi.org/10.1073/pnas.0937635100.

[59] N. Beckouche, M. Bignon, V. Lelarge, T. Mathivet, C. Pichol-Thievend, S. Berndt, J. Hardouin, M. Garand, C. Ardidie-Robouant, A. Barret, G. Melino, H. Lortat-Jacob, L. Muller, C. Monnot, S. Germain, The interaction of heparan sulfate proteoglycans with endothelial transglutaminase-2 limits VEGF165-induced angiogenesis, Sci Signal. 8 (2015) ra70. https://doi.org/10.1126/scisignal.aaa0963.

[60] M. Kerschnitzki, P. Kollmannsberger, M. Burghammer, G.N. Duda, R. Weinkamer, W. Wagermaier, P. Fratzl, Architecture of the osteocyte network correlates with bone material quality, J. Bone Miner. Res. 28 (2013) 1837–1845. https://doi.org/10.1002/jbmr.1927.

[61] I. Arganda-Carreras, R. Fernández-González, A. Muñoz-Barrutia, C. Ortiz-De-Solorzano, 3D reconstruction of histological sections: Application to mammary gland tissue, Microsc. Res. Tech. 73 (2010) 1019–1029. https://doi.org/10.1002/jemt.20829.

[62] M.M. Cordeiro, Z. Dong, T. Kaneko, Z. Zhang, M. Miyazawa, S. Shi, A.J. Smith, J.E. Nör, Dental pulp tissue engineering with stem cells from exfoliated deciduous teeth, J Endod. 34 (2008) 962–969. https://doi.org/10.1016/j.joen.2008.04.009.

[63] B. Salmon, C. Bardet, M. Khaddam, J. Naji, B.R. Coyac, B. Baroukh, F. Letourneur, J. Lesieur, F. Decup, D. Le Denmat, A. Nicoletti, A. Poliard, P.S. Rowe, E. Huet, S.O. Vital, A. Linglart, M.D. McKee, C. Chaussain, MEPE-derived ASARM peptide inhibits odontogenic differentiation of dental pulp stem cells and impairs mineralization in tooth models of X-linked hypophosphatemia, PLoS ONE. 8 (2013) e56749. https://doi.org/10.1371/journal.pone.0056749.

FIGURE LEGENDS

Figure 1: Generation of a microvascular network bearing perivascular recruitment.

A-B: Endothelial cells (1.5 10^6 cells/ml) were seeded in collagen hydrogels either alone and cultured in SHED conditioned medium (**A.i;** EC + SHED-CM) or co-seeded with SHED (1 10^6 cells/ml) and cultured in endothelial growth medium (**A.ii;** EC + SHED) for 4 days. Endothelial cells were either immuno-stained for CD31 or F- actin was detected using phalloidin-AlexaFluor488. Morphometric characteristics of capillary formation consisting in capillary length (**B.i**), diameter (**B.ii**) and tortuosity (**B.iii**) were measured. Three fields of view were analyzed over 260 µm thick z-stacks. Three independent experiments were performed in triplicate wells of 96-well plates each. Scale bar: 100 µm. **C:** Schematic representation of sample preparation for lightsheet microscopy. Endothelial cells (green) and SHED (red) were co-seeded in collagen before fibrillogenesis in a micro-well. After vascular network formation, hydrogels were fixed and mounted in agarose in a glass capillary. The capillary was then mounted on the sample holder and the hydrogel was pushed out for lightsheet excitation and image acquisition. **D-F**: Endothelial cells expressing GFP (green) were co-seeded with SHED expressing LifeAct-Ruby (red) in hydrogel and cultured for 4 days for capillary formation. **D**: Z-stacks of 400 images were acquired with a lightsheet microscope equipped with a 20X objective (step: 1 µm). Endothelial cells (green) self-assembled in a network (**D.ii**). SHED were color-coded in red when isolated, and in purple when recruited at the surface of the endothelial network (**D.iii**, **E, F.ii and iii**). See movie 1. Scale bar: 100 µm. **F**: Z-stacks of images were acquired at higher magnification (63X) with a Zeiss Observer-Apotome2 microscope. 3D reconstruction demonstrated lumen formation (*). See movie 2. Scale bar: 10 µm. Images were treated with Imaris for surface rendering and 3D reconstruction.

Figure 2: Expression of pericytes markers by SHED.

A-C: SHED, placenta pericyte (PlPC), vascular smooth muscle cells (VSMC) or endothelial cells (HUVEC) were seeded in culture dishes and fixed with PFA before immuno-staining of the indicated markers. Cells were stained for actin (red) (**A** and **B**) and either aSMA (**A**) or desmin (**B**) (green) or for NG2 (green) and PDGF-Rβ (red) (**C**). Nuclei were stained with DAPI (blue). Whereas SHED did not express aSMA, pericytes displayed heterogeneous expression of this marker. Both cell types expressed similarly desmin, NG2 and PDGF-Rβ, unlike HUVEC. Scale bar: 50 µm. **D**: HUVEC expressing GFP (green) and SHED expressing LifeAct-Ruby (red) were co-cultured in hydrogel before immunostaining of PDGF-Rβ (white). Nuclei were stained with DAPI (blue). Scale bar: 20 µm.

Figure 3: Characterization of SHED recruitment.

A: Schematic of morphometric analysis. Images of 3D co-culture of endothelial cells expressing GFP (green) and SHED-LifeAct-ruby (red) were 3D reconstructed and treated for surface rendering using Imaris. Schematic representation of nuclei is presented in orange. Morphology of SHED was manually assessed and distributed into either star-shape/isolated SHED (red) or

spread along capillary (purple). **B**: The distance between the centroid of SHED nuclei and the surface of the endothelial capillary was measured as described in the methods section and plotted for determination of a threshold distance (dotted line) allowing quantification of SHED perivascular recruitment. **C**: Time-lapse acquisition of SHED recruitment. Endothelial cells expressing GFP and SHED-LifeAct-Ruby were co-seeded in hydrogel in the sample holder dedicated to time-lapse acquisition (see Fig.S2). They were then cultured for three days for capillary formation in incubator before mounting in the chamber of the lightsheet microscope. Z-stacks of images were acquired (**i**) every 20 minutes for 7 hours. Images were treated with Imaris for surface rendering (**ii** to **v**), and cells were color-coded: endothelial cells (green), perivascular SHED (purple) and SHED being recruited and migrating along the capillary (white). See movie 4.

Figure 4: Regulation of SHED recruitment by the PDGF-Rβ pathway.

A: Schematic representation of the recruitment assay (**A**). Endothelial cells monolayers on Cytodex beads (**i**) were co-encapsulated with SHED in fibrin hydrogels. Co-cultures were maintained for 4 days (**ii**) before fixation and immunostaining of CD31 (green) and staining of nuclei with DAPI (red). Z-stacks of images were acquired with a Zeiss Observer-Apotome2 microscope. Formation of capillaries (**iii**) and distance of SHED nuclei (white arrows) to capillaries were quantified (**iv**). See movie 5. Scale bars: 25 (i), 200 (ii) and 50 (iv) µm. **B-G**: In order to assess the involvement of the PDFG-BB pathway, cultures were treated with Imatinib (0.2, 1 or 5 µM), heparin (22.5 µg/ml), anti-PDGF-B (20, 40 or 100 µg/ml) or PDGF-BB (10 or 100 ng/ml). Angiogenesis was assessed by quantification of total capillary length per bead (**B**), number of primary sprouts budding from beads (**C**) and diameter (**E**). Perivascular recruitment per length of capillary was also measured (**D**). Statistical analysis was performed using Anova followed by Bonferroni test (*, $p<0.05$, **, $p<0.01$, ***, $p<0.001$, ****, $p<0.0001$).

Figure 5: Deposition of collagen IV in the basement membrane.

A: Capillaries generated in hydrogel with endothelial cells expressing GFP and SHED-LifeAct-Ruby were immunostained for collagen IV. Lumen formation (* in **i**) and recruited SHED (# in **i**) were detected. The alpha2 chain of collagen IV staining was observed both at the surface of endothelial cells (**i**) and ensheathing perivascular cells (yellow arrows in **ii**). See movie 6. **B**: Monolayer of SHED were cultured in tissue culture dishes in their complete medium (**i**) or in endothelial medium (**ii**). Deposition of the alpha 2 chain of collagen IV in the extracellular matrix was detected by immunofluorescence. Scale bars : 20 µm.

Figure 6: Analysis of *in vivo* vascularization.

Vascularization was analyzed 30 days post-implantation in tissue constructs seeded with SHED alone or endothelial cells alone cultured in SHED conditioned medium (EC + SHED-CM) or with SHED and endothelial cells (EC + SHED). **A-B:** Athymic nude mice (n=15) were injected with an intravascular contrast agent. Reconstructed micro-CT data show vessels (red) inside the tooth slice (white) were quantified (**B**) *; P<0,05. **C-D:** vWF immunostaining was performed (**C**) and

area of vessels inside the construct (dotted line) was quantified using ImageJ (**D**). n=6 constructs per group. *: P<0.05, ***: P<0.001. Scale bar: 100 µm. **E-G:** Podocalyxin immunostaining (red) was performed (**E**) and area of vessels inside the construct (dotted line) was quantified using Image J (**F**). Nuclei were stained with DAPI (blue). n=8 constructs per group ***: P<0.001. Autofluorescent red blood cells were observed inside the lumen of human capillaries in the construct co-seeded with SHED and endothelial cells seeded with stained for podocalyxin (**G**)**.** Scale bar: 50 µm.

Figure 7: Vessel basement membrane, apoptosis and sensitive innervation.

Analysis was performed 30 days post-implantation in tissue constructs seeded with SHED alone or endothelial cells cultured in SHED conditioned medium (EC + SHED-CM) or with SHED and endothelial cells (EC + SHED). **A:** Podocalyxin (red) and collagen IV (green) immunostaining were performed. Boarders of the tissue construct are depicted (dotted line). Nuclei were stained with DAPI (blue). Boxed picture shows zoomed area. Scale bars: 100 µm, and 30 µm in boxed area. **B-C:** TUNEL assay was performed (green). Nuclei were stained with DAPI (blue). The relative apoptosis was quantified inside the construct using ImageJ (**C**). n=7 blocs per group. Scale bar: 50 µm. **D-E:** CGRP immunostaining (red) was performed showing sensory fibers in all the groups. Nuclei were stained with DAPI (blue). Sensitives fibers (white arrows) were quantified inside calibrated area using ImageJ. n=5 samples per group. Scale bars: 20 µm. *P<0.05; ***: P<0.001; ****P<0.0001.

FIGURE 1

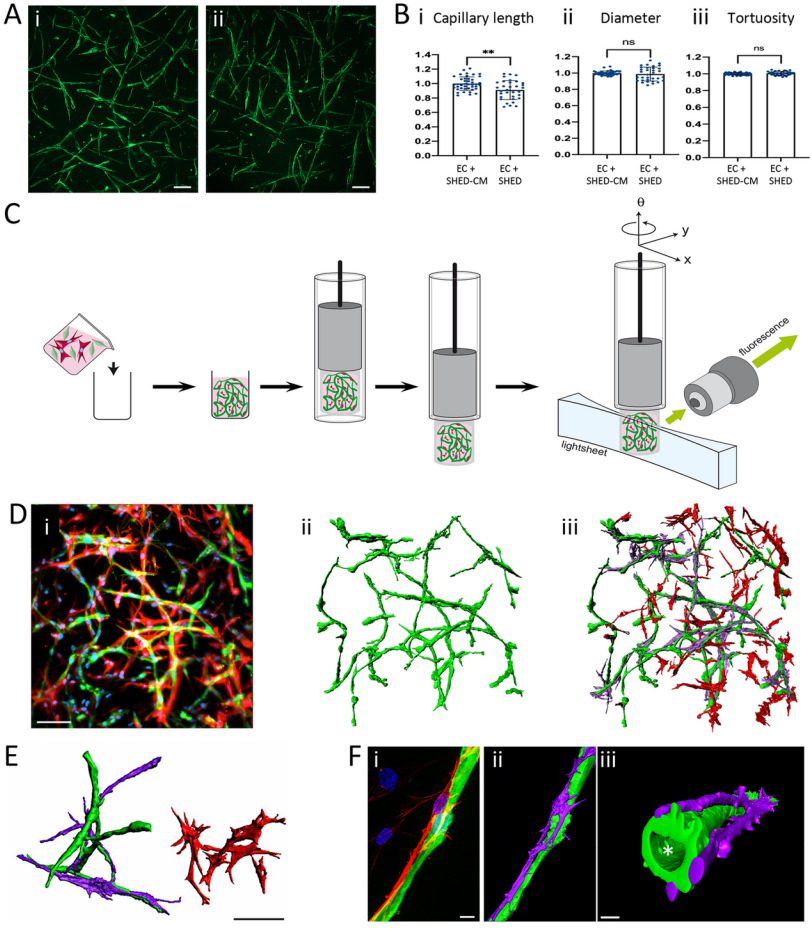
A
i
ii
B
i Capillary length
ii Diameter
iii Tortuosity
**
ns
ns
1.4
1.2
1.0
0.8
0.6
0.4
0.2
0.0
EC + SHED-CM
EC + SHED
C
θ
y
x
fluorescence
lightsheet
D
i
ii
iii
E
F
i
ii
iii
*

FIGURE 2

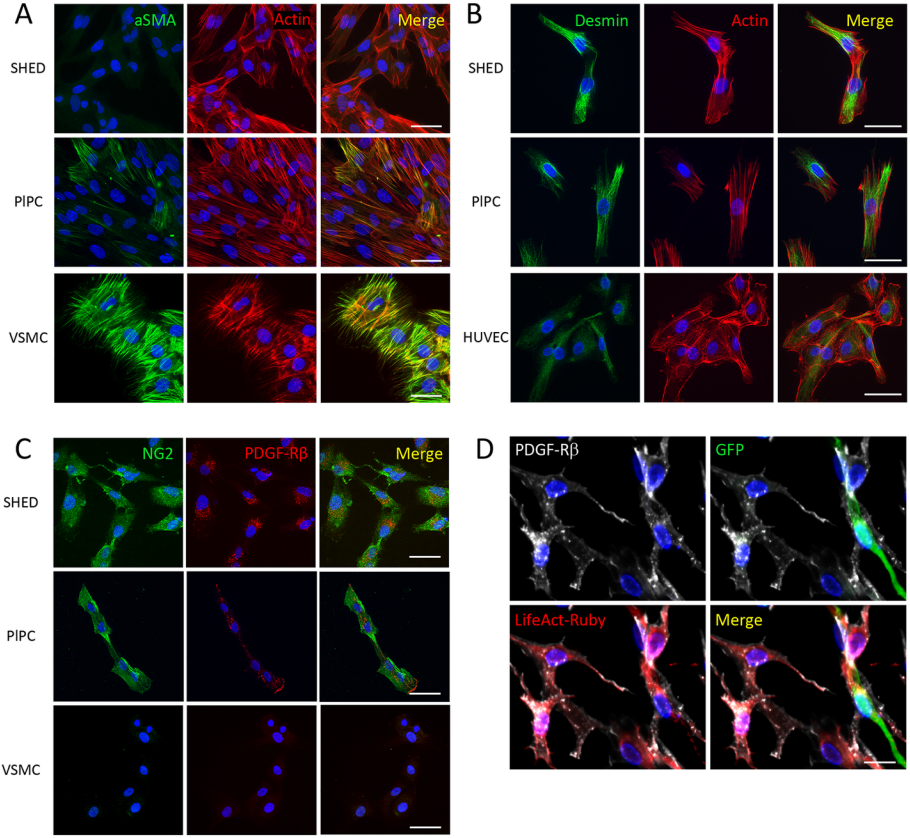
A
aSMA
Actin
Merge
SHED
PIPC
VSMC
B
Desmin
Actin
Merge
SHED
PIPC
HUVEC
C
NG2
PDGF-Rβ
Merge
SHED
PIPC
VSMC
D
PDGF-Rβ
GFP
LifeAct-Ruby
Merge

FIGURE 3


A

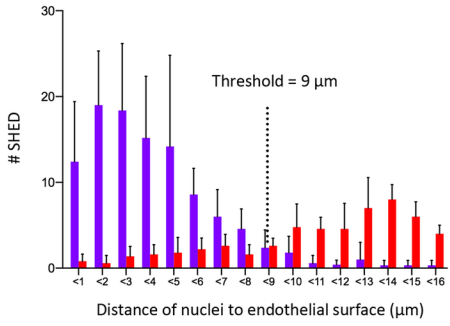
B
30
20
10
0
# SHED
Threshold = 9 µm
<1
<2
<3
<4
<5
<6
<7
<8
<9
<10
<11
<12
<13
<14
<15
<16
Distance of nuclei to endothelial surface (µm)

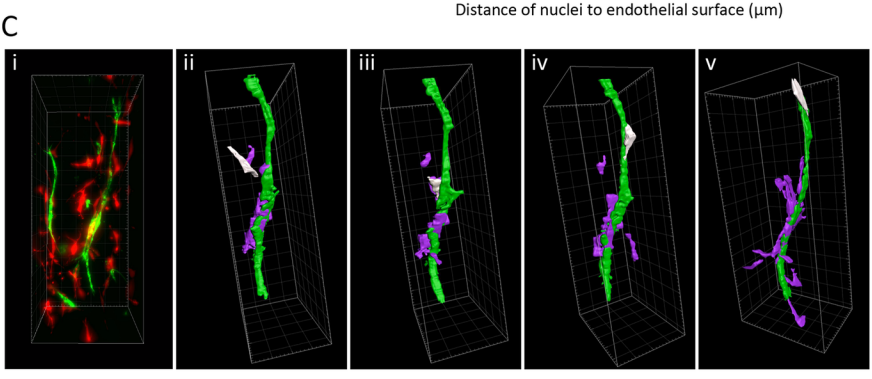
C
i
ii
iii
iv
v

FIGURE 4

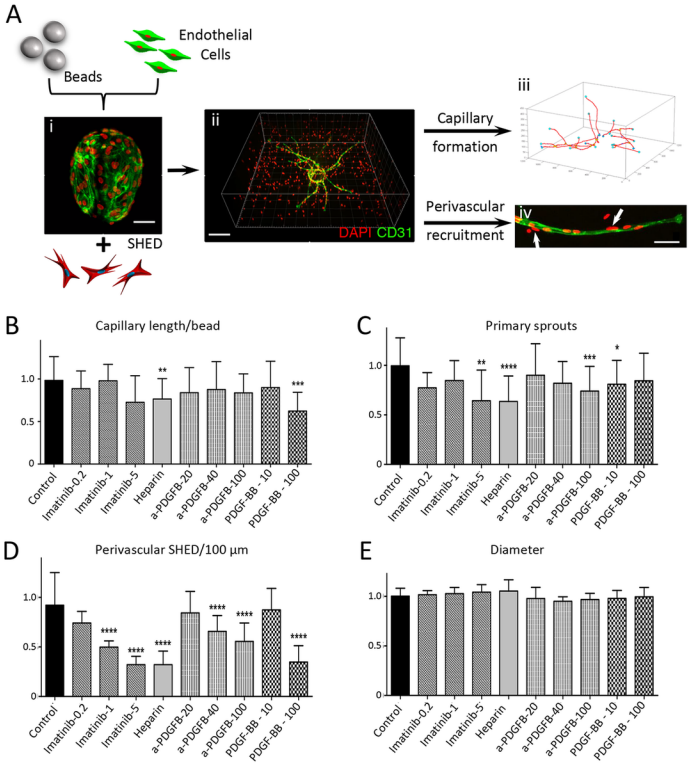
A
Endothelial Cells
Beads
i
ii
iii
iv
Capillary formation
Perivascular recruitment
DAPI CD31
SHED
B
Capillary length/bead
C
Primary sprouts
D
Perivascular SHED/100 µm
E
Diameter
Control
Imatinib-0.2
Imatinib-1
Imatinib-5
Heparin
a-PDGFB-20
a-PDGFB-40
a-PDGFB-100
PDGF-BB - 10
PDGF-BB - 100

FIGURE 5

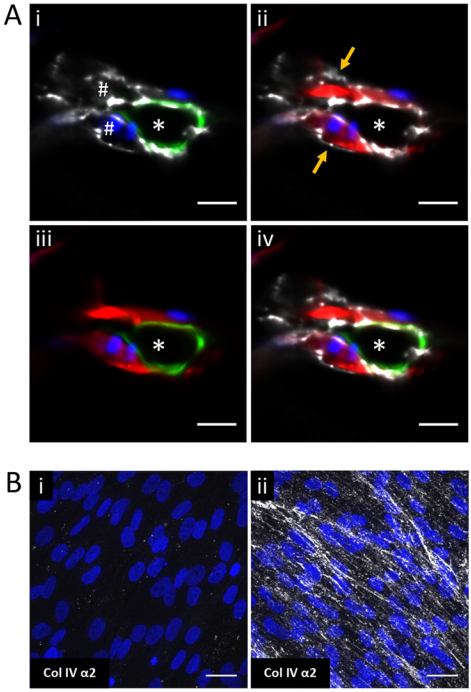

FIGURE 6

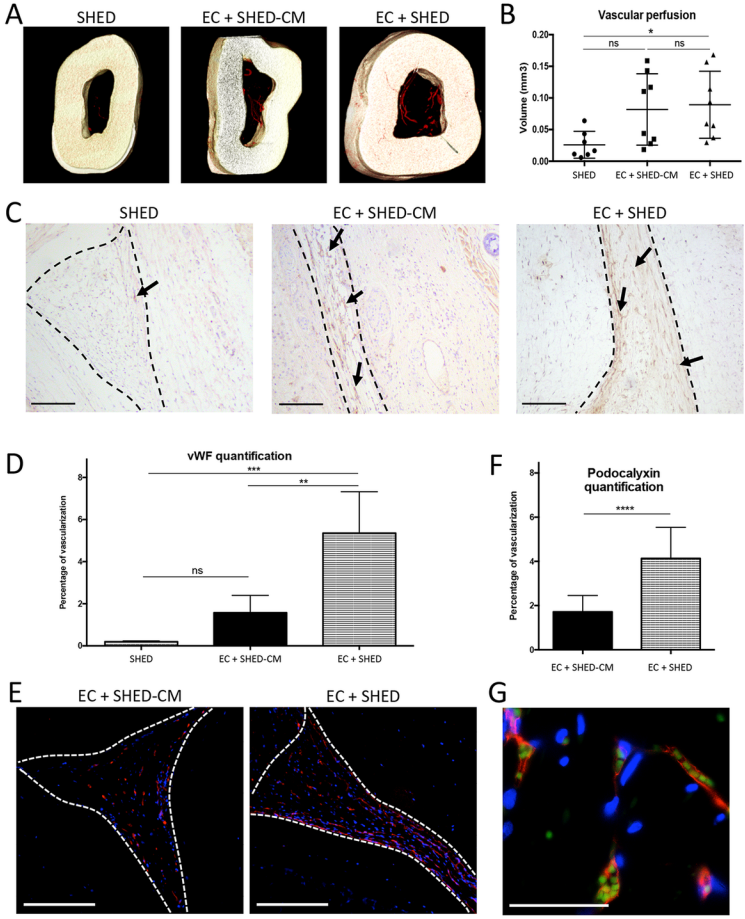
A
SHED
EC + SHED-CM
EC + SHED
B
Vascular perfusion
Volume (mm3)
0.20
0.15
0.10
0.05
0.00
ns
*
ns
SHED
EC + SHED-CM
EC + SHED
C
SHED
EC + SHED-CM
EC + SHED
D
vWF quantification
Percentage of vascularization
***
**
ns
8
6
4
2
0
SHED
EC + SHED-CM
EC + SHED
F
Podocalyxin quantification
Percentage of vascularization
****
8
6
4
2
0
EC + SHED-CM
EC + SHED
E
EC + SHED-CM
EC + SHED
G

FIGURE 7

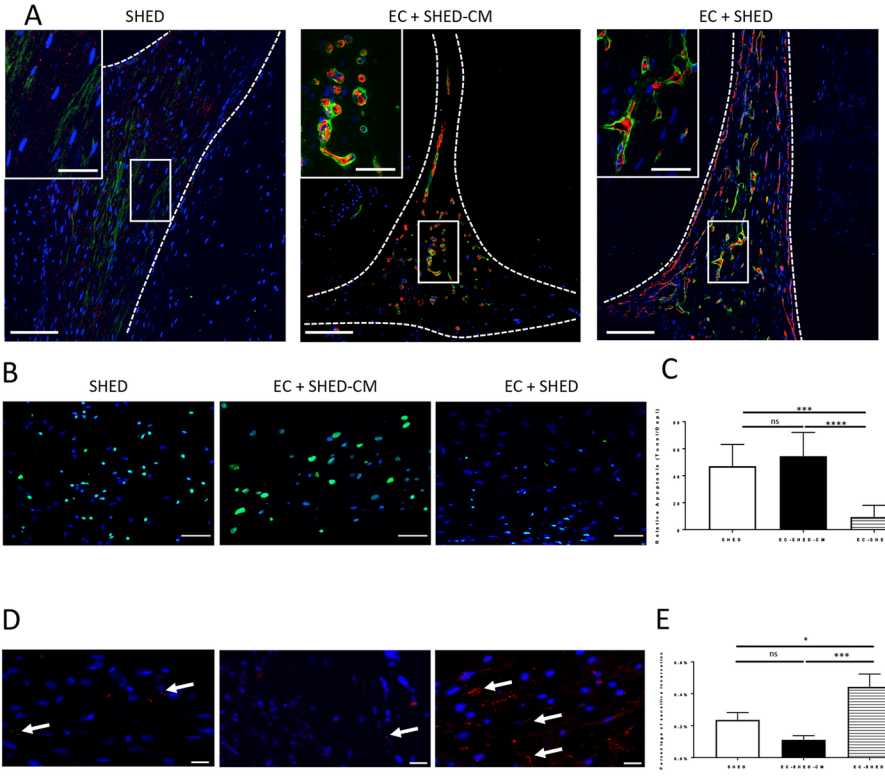
A
SHED
EC + SHED-CM
EC + SHED
B
SHED
EC + SHED-CM
EC + SHED
C
***
ns
****
SHED
EC-SHED-CM
EC-SHED
D
E
*
ns
***
SHED
EC-SHED-CM
EC-SHED